

Roles of heating and helicity in ultrafast all-optical magnetization switching in TbFeCo

LU, Xangyang, ZOU, Xiao, HINZKE, Denise, LIU, Tao, WANG, Yichuan, CHENG, Tuyan, WU, Jing, OSTLER, Thomas <<http://orcid.org/0000-0002-1328-1839>>, CAI, Jianwang, NOWAK, Ulrich, CHANTRELL, Roy, ZHAI, Ya and XU, Yongbing

Available from Sheffield Hallam University Research Archive (SHURA) at:

<https://shura.shu.ac.uk/22051/>

This document is the Published Version [VoR]

Citation:

LU, Xangyang, ZOU, Xiao, HINZKE, Denise, LIU, Tao, WANG, Yichuan, CHENG, Tuyan, WU, Jing, OSTLER, Thomas, CAI, Jianwang, NOWAK, Ulrich, CHANTRELL, Roy, ZHAI, Ya and XU, Yongbing (2018). Roles of heating and helicity in ultrafast all-optical magnetization switching in TbFeCo. *Applied Physics Letters*, 113 (3), 032405. [Article]

Copyright and re-use policy

See <http://shura.shu.ac.uk/information.html>

Roles of heating and helicity in ultrafast all-optical magnetization switching in TbFeCo

Xianyang Lu, Xiao Zou, Denise Hinzke, Tao Liu, Yichuan Wang, Tuyuan Cheng, Jing Wu, Thomas A. Ostler, Jianwang Cai, Ulrich Nowak, Roy W. Chantrell, Ya Zhai, and Yongbing Xu

Citation: *Appl. Phys. Lett.* **113**, 032405 (2018); doi: 10.1063/1.5036720

View online: <https://doi.org/10.1063/1.5036720>

View Table of Contents: <http://aip.scitation.org/toc/apl/113/3>

Published by the [American Institute of Physics](#)



The image shows a Lake Shore Measure Ready 155 Precision I/V Source. The device is a compact, silver-colored unit with a large color display on the left side. The display shows 'AC Peak Amplitude 10.0000 mV', 'Frequency 100.000 kHz', and 'DC Offset 0.0000 mV'. To the right of the display are several control buttons and a set of four colored terminals (red, green, blue, and black) for connecting test leads. The Lake Shore logo is visible in the top left corner of the device's face.

Lake Shore
CRYOTRONICS

Measure Ready
155 Precision I/V Source

A new current & voltage source
optimized for scientific research

LEARN MORE 

Roles of heating and helicity in ultrafast all-optical magnetization switching in TbFeCo

Xianyang Lu,^{1,2} Xiao Zou,¹ Denise Hinzke,³ Tao Liu,⁴ Yichuan Wang,^{1,2} Tuyuan Cheng,⁵ Jing Wu,^{1,2,a)} Thomas A. Ostler,^{6,7} Jianwang Cai,^{4,b)} Ulrich Nowak,³ Roy W. Chantrell,¹ Ya Zhai,^{5,8} and Yongbing Xu^{2,5,c)}

¹Department of Physics, University of York, York YO10 5DD, United Kingdom

²York-Nanjing International Joint Center in Spintronics, School of Electronic Science and Engineering, Nanjing University, Nanjing 210093, China

³Fachbereich Physik, Universität Konstanz, 78457 Konstanz, Germany

⁴Institute of Physics, Chinese Academy of Sciences, Beijing 100190, China

⁵Spintronics and Nanodevice Laboratory, Department of Electronics, University of York, York YO10 5DD, United Kingdom

⁶Faculty of Arts, Computing, Engineering and Sciences, Sheffield Hallam University, Sheffield S1 1WB, United Kingdom

⁷Département de Physique, L'Université de Liège, B-4000 Liège, Belgium

⁸Department of Physics, Southeast University, Nanjing 210096, China

(Received 18 April 2018; accepted 5 July 2018; published online 18 July 2018)

Using the time-resolved magneto-optical Kerr effect method, helicity-dependent all-optical magnetization switching (HD-AOS) is observed in ferrimagnetic TbFeCo films. Our results reveal the individual roles of the thermal and nonthermal effects after a single circularly polarized laser pulse. The evolution of this ultrafast switching occurs over different time scales, and a defined magnetization reversal time of 460 fs is shown—the fastest ever observed. Micromagnetic simulations based on a single macro-spin model, taking into account both heating and the inverse Faraday effect, are performed which reproduce HD-AOS demonstrating a linear path for magnetization reversal. Published by AIP Publishing. <https://doi.org/10.1063/1.5036720>

Since the demonstration of magnetization reversal by a single femtosecond laser pulse in 2007,¹ the field of all-optical switching (AOS) has been extensively studied both theoretically and experimentally. The AOS of the magnetisation in the ferrimagnetic alloy, GdFeCo (the initially investigated material for AOS), has been shown to be established through a purely thermal effect^{2–5} where the dynamics of the magnetisation reversal proceed via a transient ferromagnetic-like state.^{6,7} Very recently, ultrafast electronic heat currents have been shown experimentally to be sufficient to switch the magnetization in this same material,^{8,9} which provides further evidence of the thermal origins of AOS in GdFeCo.¹⁰ Consequently, AOS in GdFeCo is almost independent of the laser helicity of the laser pulse, which is named helicity-independent AOS (HI-AOS).

On the other hand, there are many examples of AOS observed in other materials, which are strongly helicity dependent, e.g., ferromagnetic Co/Pt multilayers,¹¹ FePt nanoparticles,¹² synthetic ferrimagnetic heterostructures,¹³ and Tb-based ferrimagnets.^{14–16} For these materials, there is a one-to-one correspondence of the helicity of the laser light control and the magnetization orientation, deemed helicity dependent AOS (HD-AOS). A dependence on helicity was observed in GdFeCo for single pulses applied to the alloy for a narrow range of fluence,¹⁷ which was quantitatively explained as arising from magnetic circular dichroism (MCD).¹⁸ Besides the purely thermal effect and MCD,¹⁹ other mechanisms have been proposed to

explain the observed AOS, e.g., inverse Faraday effect (IFE),^{1,20–22} stimulated Raman scattering,^{23,24} sublattice exchange relaxation,²⁵ ultrafast exchange scattering,²⁶ and optical spin pumping.²⁷ However, the underlying physics of HD-AOS in a larger variety of materials is still unclear, especially of the roles of the helicity and thermal effects of the laser pulse. Several experimental criteria and models have been proposed to interpret HD-AOS. A so-called low-remnance criterion was reported whereby HD-AOS is only obtained below a magnetization remanence threshold of 220 emu/cm³ for several materials.¹⁵ Recently, a domain size criterion for the observation of HD-AOS has been proposed, whereby the laser spot size should be smaller than the equilibrium size of magnetic domains formed during the cooling process after laser irradiation.²⁸ Meanwhile, using a time-dependent anomalous Hall effect technique, HD-AOS has been demonstrated to consist of a steplike helicity-independent multiple-domain formation followed by a helicity-dependent remagnetization.²⁹ There have been several models of optical switching presented in the literature, as well as differing measurements with different conclusions as to the importance of the thermal or nonthermal effects.^{4,17,19,30,31} In this context, one intuitive question is can the contributions of both thermal and nonthermal effects be quantified simultaneously during a single circularly polarized laser pulse? The ultrafast laser-induced demagnetization is well-known to have a thermal aspect;³² however, there will inevitably be some contribution from both thermal and nonthermal effects during one single laser pulse. However, in all the Kerr or Faraday image detections, it is impossible to measure both of these two effects because only the final static magnetization states are observed – one requires access to temporal information.

^{a)}Email: jing.wu@york.ac.uk

^{b)}Email: jwcai@iphy.ac.cn

^{c)}Email: yongbing.xu@york.ac.uk

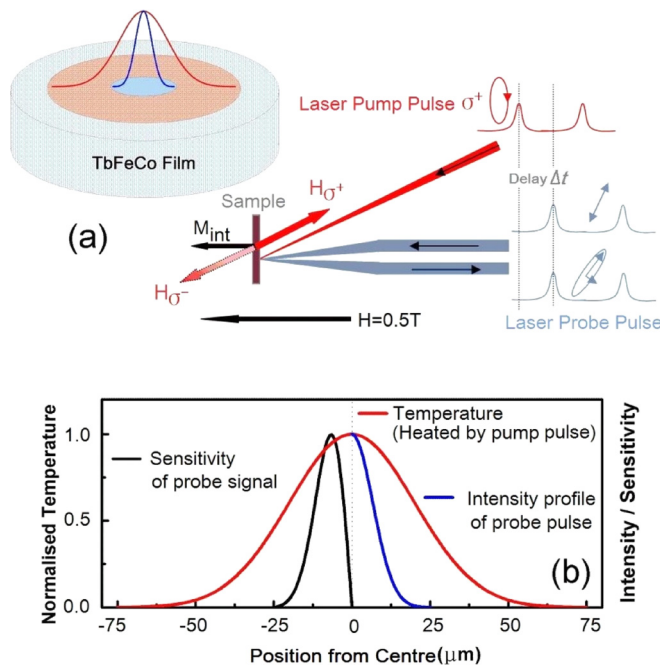


FIG. 1. (a) A schematic diagram of the experimental set-up with a bias field of $H = 0.5$ T. H_{σ^+} represents the effective field of the pump pulse with σ^+ polarization (red line) due to the IFE. (b) The normalized radial sensitivity of Kerr rotation (only left half shown for clarity) and temperature distribution across the pump spot together with the intensity profile of the probe spot (only right half shown for clarity).

To explore the roles of the thermal and non-thermal effects in HD-AOS and the time scales in this process, we used the laser pump-probe technique, also known as the time-resolved magneto-Kerr effect measurement (Fig. 1)³³ (details in the [supplementary material](#)), to measure the transient magnetization change after a single laser pulse acting on TbFeCo. The transient reflectivity change is simultaneously monitored. TbFeCo is a similar ferrimagnet compared to GdFeCo as the Tb sublattice is antiferromagnetically coupled with the FeCo sublattice,^{30,34,35} forming a ferrimagnetic structure. However, because of the large difference between the

spin-orbit coupling of Tb and Gd,³⁶ Gd- and Tb-based alloys show different spin dynamics as well as distinct switching mechanisms.^{37,38}

In order to separate thermal and nonthermal contributions, time domain measurements are performed, varying the laser pump fluence and helicity, whilst keeping the direction of the external magnetic field fixed in the direction almost parallel to the direction of the induced magnetization due to the σ^- helicity pulses (and nearly anti-parallel in the σ^+ case). The transient Kerr rotation obtained under different laser fluences with different laser helicities is shown in Figs. 2(a)–2(c). Between the two lower laser fluences (2.8 and 5 mJ/cm²), the dynamic responses are very similar except that the amplitude is increased with the laser fluence. The two curves taken with different laser helicities converge after around 240 fs time delay, suggesting that only thermal effects exist for these laser fluences because the thermal effects are insensitive to the laser helicity while the nonthermal effect is.³¹ The peaks around zero delay are the so-called specular inverse Faraday effect (SIFE) and specular optical Kerr effect (SOKE) contributions,³⁹ as detailed in Fig. S1 in the [supplementary material](#). However, as the laser fluence is increased to 9 mJ/cm², the two curves taken with different laser helicities no longer converge. The curve excited by laser pulses of σ^+ polarization (a helicity that induces an effective field opposite to the external magnetic field) switches further away from the initial magnetization direction compared to the curve excited by σ^- polarised laser pulses. This extra switching starts at around $t_3 = 240$ fs, indicating the onset of the nonthermal effect. The time evolution of the reflectivity has also been investigated, indicating a peak electron temperature at approximately $t_1 = 70$ fs. There is no obvious laser helicity dependence in the reflectivity which can be seen from the data taken at 9 mJ/cm² as shown in Fig. 2(d). In this case, the absorption of light is at the same level as well as the electron temperature profiles, which means that there is no significant MCD effect. The oscillations with a high frequency of 42 GHz shown in both the

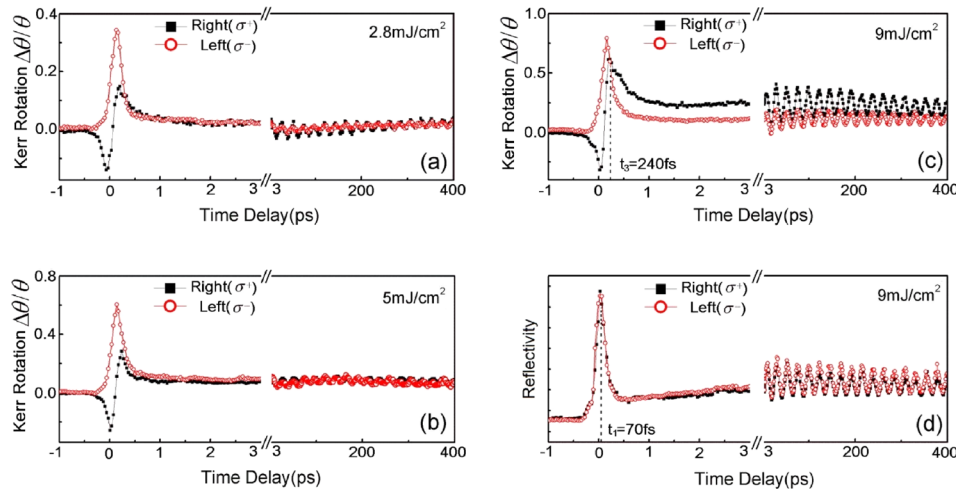


FIG. 2. (a) and (b) show the time domain Kerr rotation taken under pump fluences of 2.8 and 5 mJ/cm², respectively. (c) presents the time domain Kerr rotation obtained under a pump beam fluence of 9 mJ/cm². At about 240 fs time delay, the curve excited by pump pulses of σ^+ polarization (black solid squares) starts to switch further away from the initial magnetization direction compared with the curve excited by σ^- polarized (red hollow dots) pump pulses. (d) shows the time domain reflectivity data at 9 mJ/cm² for both σ^+ and σ^- polarizations. The two curves overlap with the peak at $t_1 = 70$ fs, indicating the maximal electron temperature.

transient Kerr rotation and reflectivity data have no magnetic field dependence. Therefore, it may be originated from a laser-induced strain-wave in the amorphous films (details in the [supplementary material](#)).

The thermal and nonthermal effects on the magnetization can be separated by analysing the sum and difference of the experimental data under different laser helicities, respectively. Therefore, the datasets in Figs. 2(a)–2(c) have been analysed accordingly and are presented in Figs. 3(a) and 3(b). The difference data in Fig. 3(a) show the time evolution of the nonthermal effect. For the two cases with lower laser fluence, the time evolution of the two difference data overlaps and goes back to its original state immediately after the SIFE/SOKE peak, giving no indication of any nonthermal effect. As the pump fluence is increased to 9 mJ/cm², the difference signal does not return to the original state immediately. Instead, it keeps increasing to its maximum magnitude at around $t_4 = 460$ fs time delay showing that the magnetization has partially switched in some regions of the irradiated area to a different magnetization state. This demonstrates unambiguously a helicity-dependent switching in TbFeCo triggered at close to $t_3 = 240$ fs and magnetization re-orientation at approximately $t_4 = 460$ fs after circularly polarized laser excitation.

Figure 3(b) presents the time evolution of the directly measured heat-driven dynamics excited by a linearly polarized laser of the same energy, along with the data obtained by taking the sum of the σ^+ and σ^- cases for three different laser fluences. All three pairs of time domain Kerr rotation data reach maxima around $t_2 = 160$ fs, indicating the time scale of the quenching of the magnetic order. Two pairs of time domain data taken at lower laser fluence overlap with

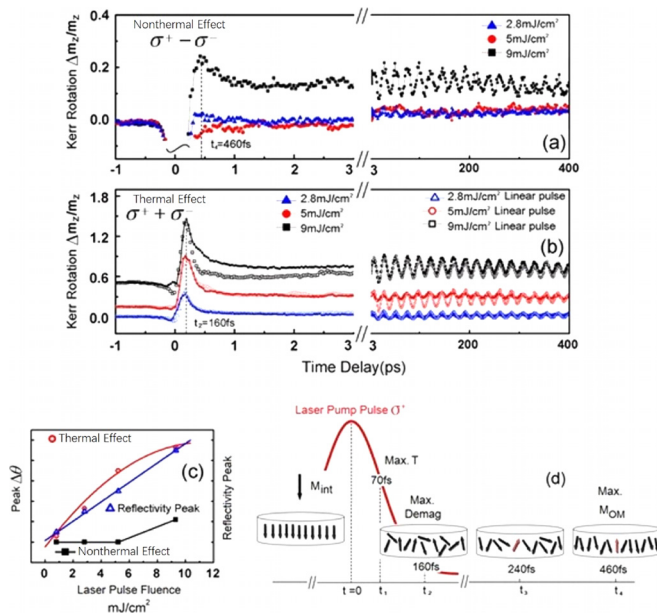


FIG. 3. (a) shows the difference between the σ^+ and σ^- pump pulses as a function of time. (b) The three solid curves show the sum of the σ^+ and σ^- pump pulses with time. The hollow curves are time domain responses excited by the linearly polarized laser pulse at the same pump fluences. (c) The peak amplitude of the thermal effect (red circles), of the reflectivity (blue triangles), and of the nonthermal effect (black squares) at a delay time of 460 fs as a function of the pump fluence. (d) shows a schematic diagram of the ultrafast process induced at a pump fluence of 9 mJ/cm².

each other extremely well since the SIFE/SOKE changes phase between σ^+ and σ^- helicities and are thus cancelled out by the sum operation. The pair taken at 9 mJ/cm² starts to diverge from each other immediately after the maximum demagnetization with the sum data deviating further from the initial magnetization state, indicating the onset of the helicity-dependent switching excited by σ^+ pump pulses, which are more profound than those excited by σ^- pump pulses. This is expected since the helicity-dependent switching induced by two different laser helicities is different in phase as well as in magnitude, depending on the instantaneous magnetization state, and also supported by our theoretical calculations shown below. The peak amplitude of the thermal and reflectivity data is plotted as a function of the pump laser fluence in Fig. 3(c) together with the amplitude of the nonthermal data at 460 fs time delay. Figure 3(c) shows that the electron temperature is proportional to the laser fluence; the sample is nearly totally demagnetized at 9 mJ/cm² which is consistent with the condition required for helicity-dependent switching;²⁹ there is no sign of helicity-dependent switching for the data taken at lower pump fluence. Note that 9 mJ/cm² is the highest pump fluence, which can be applied without damaging the sample surface, and the helicity-dependent switching is only observed at this highest pump fluence. The whole ultrafast process induced at a pump fluence of 9 mJ/cm² is schematically summarized in Fig. 3(d). The electron temperature reaches its maximum at 70 fs time delay, and the magnetic order is largely quenched by 160 fs. The onset of helicity-dependent switching takes place within 240 fs, and a new magnetization direction is defined by 460 fs.

To understand the observed time domain results of HD-AOS, two main effects are considered, namely, the MCD¹⁸ and the IFE.²⁰ MCD leads to a different absorption of the two circular helicities in the different domains and it is excluded because from the transient reflectivity curves, no difference is observed with respect to the laser helicity. In Ref. 12, the magnetization induced through the IFE effect was directly calculated for the case of FePt with *ab-initio* methods.⁴⁰ In our simulations, due to a lack of *ab-initio* calculations for the considered TbFeCo alloy, this temporal change of the magnetization caused by the IFE is assumed to be due to an effective magnetic field.^{17,41} Our simulations are based on a single macro-spin model whereby we solve the Landau-Lifshitz-Bloch (LLB) equation numerically.^{42–46} The LLB equation takes into account transient changes in the length of the magnetization required to describe the heating from the laser pulse. All our methods are described in detail in Ref. 44 and also summarized in the [supplementary material](#). The results of these simulations are shown in Figs. 4(a)–4(d) for different peak electron temperatures T_e , corresponding to different laser fluences, as summarised in Figs. 4(e) and 4(f). The figure focuses on the change in the reduced magnetization (M/M_s) along the easy-axis at short time-scales. Starting at room temperature, the reduced magnetization at equilibrium is around 0.8. Complete demagnetization can be achieved within 300 fs, and magnetization reversal can be triggered on the sub-picosecond time-scale for higher T_e . The theoretical model reproduces the sub-picosecond reversal observed experimentally and confirms

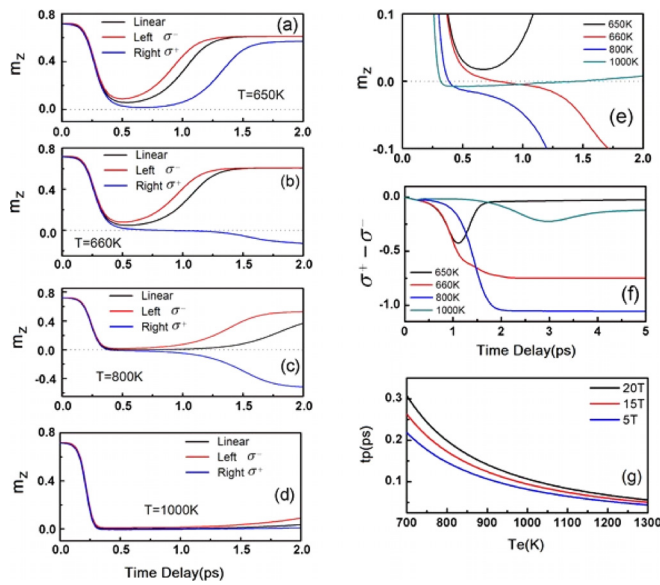


FIG. 4. (a)–(d) Simulated magnetic response for increasing peak electron temperatures showing the onset of magnetization reversal. Reversal occurs at around 660 K, where the linear reversal mechanism sets in. At higher temperatures (d), the magnetization is destroyed after reversal. (e) Magnetic response for different values of the peak electron temperature. (f) Shows the difference in the response to the difference helicities. Optically induced reversal is demonstrated at 660 and 800 K. The onset of reversal depends critically on the onset of linear reversal. The response time calculated from Eq. (S2) demonstrates that the predicted reversal takes place on the sub-picosecond timescale, consistent with the experimental results. (g) Minimal field and temperature pulse time needed to trigger a magnetization reversal taken from Eq. (S2).

the above interpretation of the experimental data. Above all, the reversal occurs only above a critical temperature corresponding to that of the linear reversal model; reversal on this timescale cannot occur via precessional mechanisms, which occur on the nanosecond timescale. Therefore, the peak electron temperature plays a significant role in HD-AOS. In Ref. 47, an analytical formula was derived for the minimal pulse time (in terms of rectangular field and temperature pulses), which is needed to switch the sign of the magnetization [see Eq. (S2) in the [supplementary material](#)]. It is illustrated in Fig. 3(g). We noticed that in the simulations, the switching times are slightly larger than with the analytical formula. This is due to the fact that for the analytical formula, rectangular temperature and field pulses are assumed, while in the simulations, more realistic profiles are calculated. We also note that the simulations further predict a rapid increase in the magnetization in a negative sense after reversal, whereas the experimental data indicate that the magnetization recovers towards the original value. We attribute this to the simplified nature of the calculations, which are based on a single spin, whereas the experimental sample has a large-scale domain structure, though quantitative agreement is not the aim here. While the reversal of the magnetization via the linear reversal mechanism is unlikely to be affected by the domain structure, it is reasonable to expect that the magnetization measured by the probe beam after the pulse cannot be simulated within the current single spin model. Furthermore, multi-macrospin calculations would most likely still not be comparable with experimental measurements as the size of the probe beam is still many micrometres and likely beyond the size of this type

of simulation. It should also be noticed that, compared to the current single macrospin simulations leading to a linear reversal mechanism, an atomistic spin approach would possibly give a different picture, as there would be more degrees of freedom for the atomic spins to relax.

In summary, the HD-AOS is unambiguously demonstrated in a TbFeCo film by one single circularly polarized laser pulse. The thermal and nonthermal effects are seen to have different time scales, respectively. High pump fluences are required to observe laser helicity effects, which is consistent with other reported works.^{28,29} Note that the effect of heat accumulation is not excluded in our measurements, but the 1 kHz laser repetition rate is much lower than the repetition rate used in Ref. 15 which shows no significant accumulative heat. Besides, the relaxation time of transient reflectivity response is quite small in our measurements, so the effect of accumulative heat should not play a role. The interplay between laser heating and helicity is stimulated by a single laser pulse. The whole process of the magnetization switching consists of four phases: peak electron temperature is achieved; the system becomes fully demagnetized; magnetization switching is triggered; and a new magnetization direction is defined. Furthermore, from our measurements, we can see that, on the sub-picosecond time-scales, there is a magnetization switching time within 460 fs—the fastest among the reported times in the literature.^{17,41,48,49} Very recently, a theoretical study by means of first-principles and model simulation predicts a magnetization switching time of 218 fs ~609 fs,⁵⁰ which is in good agreement with our findings. This sub-picosecond switching is reproduced using a single macro-spin model based on the stochastic Landau-Lifshitz-Bloch equation, confirming the linear reversal mechanism without spin precession in all-optically induced magnetization switching in TbFeCo. Also, the simulations suggest that heating the electron system to a critical temperature may play an important role in this kind of magnetization reversal. Above all, the finding of ultrafast helicity-dependent all-optical magnetization switching in a high anisotropy system triggered by a single laser pulse brings all-optical magnetic recording a major step closer to high data rate and high data density applications.

See [supplementary material](#) for details of sample preparation, polar time-resolved magneto-optical Kerr effect (TR-MOKE) setup, probe sensitivity, and theoretical modelling. The SIFE/SOKE contribution and the strain waves are also presented.

This work was supported in part by the National Basic Research Program of China (No. 2014CB921101), the National Key Research and Development Program of China (No. 2016YFA0300803), the National Natural Science Foundation of China (No. 61427812, 11574137, 11774160), Jiangsu Shuangchuang Programme, and the Natural Science Foundation of Jiangsu Province of China (No. BK20140054). T. A. Ostler gratefully acknowledges the support of the Marie Curie incoming BeIPD-COFUND Fellowship Program at the University of Liège.

¹C. D. Stanciu, F. Hansteen, A. V. Kimel, A. Kirilyuk, A. Tsukamoto, A. Itoh, and T. Rasing, *Phys. Rev. Lett.* **99**, 047601 (2007).

- ²J. Y. Chen, L. He, J. P. Wang, and M. Li, *Phys. Rev. Appl.* **7**, 021001 (2017).
- ³T. A. Ostler, J. Barker, R. F. L. Evans, R. W. Chantrell, U. Atxitia, O. Chubykalo-Fesenko, S. El Moussaoui, L. Le Guyader, E. Mengotti, L. J. Heyderman, F. Nolting, A. Tsukamoto, A. Itoh, D. Afanasiev, B. A. Ivanov, A. M. Kalashnikova, K. Vahaplar, J. Mentink, A. Kirilyuk, T. Rasing, and A. V. Kimel, *Nat. Commun.* **3**, 666 (2012).
- ⁴A. Kirilyuk, A. V. Kimel, and T. Rasing, *Rep. Prog. Phys.* **76**, 026501 (2013).
- ⁵R. Chimata, L. Isaeva, K. Kádas, A. Bergman, B. Sanyal, J. H. Mentink, M. I. Katsnelson, T. Rasing, A. Kirilyuk, A. Kimel, O. Eriksson, and M. Pereiro, *Phys. Rev. B* **92**, 094411 (2015).
- ⁶I. Radu, K. Vahaplar, C. Stamm, T. Kachel, N. Pontius, H. A. Dürr, T. A. Ostler, J. Barker, R. F. L. Evans, R. W. Chantrell, A. Tsukamoto, A. Itoh, A. Kirilyuk, T. Rasing, and A. V. Kimel, *Nature (London)* **472**, 205 (2011).
- ⁷S. Wienholdt, D. Hinzke, K. Carva, P. M. Oppeneer, and U. Nowak, *Phys. Rev. B* **88**, 020406 (2013).
- ⁸R. B. Wilson, J. Gorchon, Y. Yang, C.-H. Lambert, S. Salahuddin, and J. Bokor, *Phys. Rev. B* **95**, 180409 (2017).
- ⁹Y. Xu, M. Deb, G. Malinowski, M. Hehn, W. Zhao, and S. Mangin, *Adv. Mater.* **29**, 1703474 (2017).
- ¹⁰U. Atxitia, T. A. Ostler, R. W. Chantrell, and O. Chubykalo-Fesenko, *Appl. Phys. Lett.* **107**, 192402 (2015).
- ¹¹C.-H. Lambert, S. Mangin, B. S. D. C. S. Varaprasad, Y. K. Takahashi, M. Hehn, M. Cinchetti, G. Malinowski, K. Hono, Y. Fainman, M. Aeschlimann, and E. E. Fullerton, *Science* **345**, 1337 (2014).
- ¹²R. John, M. Bertrita, D. Hinzke, C. Müller, T. Santos, H. Ulrichs, P. Nieves, J. Walowski, R. Mondal, O. Chubykalo-Fesenko, J. McCord, P. M. Oppeneer, U. Nowak, and M. Münzenberg, *Sci. Rep.* **7**, 4114 (2017).
- ¹³S. Mangin, M. Gottwald, C.-H. Lambert, D. Steil, V. Uhlir, L. Pang, M. Hehn, S. Alebrand, M. Cinchetti, G. Malinowski, Y. Fainman, M. Aeschlimann, and E. E. Fullerton, *Nat. Mater.* **13**, 286 (2014).
- ¹⁴A. Hassdenteufel, B. Hebler, C. Schubert, A. Liebig, M. Teich, M. Helm, M. Aeschlimann, M. Albrecht, and R. Bratschitsch, *Adv. Mater.* **25**, 3122 (2013).
- ¹⁵A. Hassdenteufel, J. Schmidt, C. Schubert, B. Hebler, M. Helm, M. Albrecht, and R. Bratschitsch, *Phys. Rev. B* **91**, 104431 (2015).
- ¹⁶T. Y. Cheng, J. Wu, M. Willcox, T. Liu, J. W. Cai, R. W. Chantrell, and Y. B. Xu, *IEEE Trans. Magn.* **48**, 3387 (2012).
- ¹⁷K. Vahaplar, A. M. Kalashnikova, A. V. Kimel, S. Gerlach, D. Hinzke, U. Nowak, R. Chantrell, A. Tsukamoto, A. Itoh, A. Kirilyuk, and T. Rasing, *Phys. Rev. B* **85**, 104402 (2012).
- ¹⁸A. R. Khorsand, M. Savoini, A. Kirilyuk, A. V. Kimel, A. Tsukamoto, A. Itoh, and T. Rasing, *Phys. Rev. Lett.* **108**, 127205 (2012).
- ¹⁹J. Gorchon, Y. Yang, and J. Bokor, *Phys. Rev. B* **94**, 020409 (2016).
- ²⁰T. D. Cornelissen, R. Córdoba, and B. Koopmans, *Appl. Phys. Lett.* **108**, 142405 (2016).
- ²¹C. D. Stanciu, F. Hansteen, A. V. Kimel, A. Tsukamoto, A. Itoh, A. Kirilyuk, and T. Rasing, *Phys. Rev. Lett.* **98**, 207401 (2007).
- ²²A. V. Kimel, A. Kirilyuk, P. A. Usachev, R. V. Pisarev, A. M. Balbashov, and T. Rasing, *Nature (London)* **435**, 655 (2005).
- ²³V. N. Gridnev, *Phys. Rev. B* **77**, 094426 (2008).
- ²⁴D. Popova, A. Bringer, and S. Blügel, *Phys. Rev. B* **85**, 094419 (2012).
- ²⁵J. H. Mentink, J. Hellsvik, D. V. Afanasiev, B. A. Ivanov, A. Kirilyuk, A. V. Kimel, O. Eriksson, M. I. Katsnelson, and T. Rasing, *Phys. Rev. Lett.* **108**, 057202 (2012).
- ²⁶A. Baral and H. C. Schneider, *Phys. Rev. B* **91**, 100402 (2015).
- ²⁷V. N. Gridnev, *Phys. Rev. B* **88**, 014405 (2013).
- ²⁸M. S. El Hadri, M. Hehn, P. Pirro, C.-H. Lambert, G. Malinowski, E. E. Fullerton, and S. Mangin, *Phys. Rev. B* **94**, 064419 (2016).
- ²⁹M. S. El Hadri, P. Pirro, C.-H. Lambert, S. Petit-Watelot, Y. Quessab, M. Hehn, F. Montaigne, G. Malinowski, and S. Mangin, *Phys. Rev. B* **94**, 064412 (2016).
- ³⁰R. Moreno, T. A. Ostler, R. W. Chantrell, and O. Chubykalo-Fesenko, *Phys. Rev. B* **96**, 014409 (2017).
- ³¹A. Kirilyuk, A. V. Kimel, and T. Rasing, *Rev. Mod. Phys.* **82**, 2731 (2010); **88**, 039904 (2016).
- ³²E. Beaurepaire, J.-C. Merle, A. Daunois, and J.-Y. Bigot, *Phys. Rev. Lett.* **76**, 4250 (1996).
- ³³B. Liu, X. Ruan, Z. Wu, H. Tu, J. Du, J. Wu, X. Lu, L. He, R. Zhang, and Y. Xu, *Appl. Phys. Lett.* **109**, 042401 (2016).
- ³⁴S. Alebrand, M. Gottwald, M. Hehn, D. Steil, M. Cinchetti, D. Lacour, E. E. Fullerton, M. Aeschlimann, and S. Mangin, *Appl. Phys. Lett.* **101**, 162408 (2012).
- ³⁵A. Hassdenteufel, C. Schubert, J. Schmidt, P. Richter, D. R. T. Zahn, G. Salvan, M. Helm, R. Bratschitsch, and M. Albrecht, *Appl. Phys. Lett.* **105**, 112403 (2014).
- ³⁶M. Wietstruk, A. Melnikov, C. Stamm, T. Kachel, N. Pontius, M. Sultan, C. Gahl, M. Weinelt, H. A. Dürr, and U. Bovensiepen, *Phys. Rev. Lett.* **106**, 127401 (2011).
- ³⁷A. R. Khorsand, M. Savoini, A. Kirilyuk, A. V. Kimel, A. Tsukamoto, A. Itoh, and T. Rasing, *Phys. Rev. Lett.* **110**, 107205 (2013).
- ³⁸C. Bunce, J. Wu, G. Ju, B. Lu, D. Hinzke, N. Kazantseva, U. Nowak, and R. W. Chantrell, *Phys. Rev. B* **81**, 174428 (2010).
- ³⁹F. Dalla Longa, J. T. Kohlhepp, W. J. M. De Jonge, and B. Koopmans, *Phys. Rev. B* **75**, 224431 (2007).
- ⁴⁰M. Battiatto, G. Barbalinardo, and P. M. Oppeneer, *Phys. Rev. B* **89**, 014413 (2014).
- ⁴¹K. Vahaplar, A. M. Kalashnikova, A. Kimel, D. Hinzke, U. Nowak, R. Chantrell, A. Tsukamoto, A. Itoh, A. Kirilyuk, and T. Rasing, *Phys. Rev. Lett.* **103**, 117201 (2009).
- ⁴²D. A. Garanin and O. Chubykalo-Fesenko, *Phys. Rev. B* **70**, 212409 (2004).
- ⁴³U. Atxitia, O. Chubykalo-Fesenko, N. Kazantseva, D. Hinzke, U. Nowak, and R. W. Chantrell, *Appl. Phys. Lett.* **91**, 232507 (2007).
- ⁴⁴N. Kazantseva, D. Hinzke, U. Nowak, R. W. Chantrell, U. Atxitia, and O. Chubykalo-Fesenko, *Phys. Rev. B* **77**, 184428 (2008).
- ⁴⁵T. A. Ostler, M. O. A. Ellis, D. Hinzke, and U. Nowak, *Phys. Rev. B* **90**, 094402 (2014).
- ⁴⁶U. Atxitia, D. Hinzke, and U. Nowak, *J. Phys. D: Appl. Phys.* **50**, 033003 (2017).
- ⁴⁷N. Kazantseva, D. Hinzke, R. W. Chantrell, and U. Nowak, *EPL* **86**, 27006 (2009).
- ⁴⁸L. Le Guyader, M. Savoini, S. El Moussaoui, M. Buzzi, A. Tsukamoto, A. Itoh, A. Kirilyuk, T. Rasing, A. V. Kimel, and F. Nolting, *Nat. Commun.* **6**, 5839 (2015).
- ⁴⁹T. Ogasawara, N. Iwata, Y. Murakami, H. Okamoto, and Y. Tokura, *Appl. Phys. Lett.* **94**, 162507 (2009).
- ⁵⁰G. P. Zhang, Z. Babyak, Y. Xue, Y. H. Bai, and T. F. George, *Phys. Rev. B* **96**, 134407 (2017).